Registration of a Robotic System to a Medical Imaging System

Abhinav Gulhar[1,2], Danilo Briese[1,2], Philip W. Mewes[2] and Georg Rose[1]

Abstract— The presence of robots not only in industrial settings but also in operating rooms is increasing with advancements in technology. They are not only huge machines carrying out tedious and arduous tasks while being caged behind fences, but also work in collaboration, close proximity of, and in cooperation with humans. Image guided minimally invasive approaches to accurately navigate a robot to precise anatomical locations can be followed only once the robot is registered to the medical imaging system. In this paper, we present an approach to register a robotic system to a medical imaging system without the use of any tracking device or continuous X-ray imaging. The system consists of a lightweight robot equipped with internal torque sensors. The registration is realized by a series of landmark transformations. The robot is manually moved and guided to distinct landmarks whose positions are known in the coordinate system of the imaging system. By driving the robot to these distinct landmarks, their position relative to the coordinate system of the robotic system is also known. By comparing the respective positions of the landmarks in the two coordinate systems, both systems are registered. With 8 screws on the operating table used as landmarks for this registration, we obtain a median error of [6.9, 20.6, 18.6] mm and a standard deviation of [2.9, 2.6, 2.2] mm when compared to an X-ray based ground truth.

I. INTRODUCTION

Robots have become a solution in fields such as industrial production, laboratory automation, inspection etc. to replace numerous tasks in which the limitations of the human body such as speed and fatigue might affect results. In medical setting, robots are employed to deal with copious, detailed, quantitative information, and may provide precise and accurate results [1], [17]. Their presence in operating rooms for minimally invasive surgery (MIS) is related to their intrinsic properties such as three-dimensional spatial accuracy and their instrumental aid in enhancing surgery through improved precision and stability [5]. Combined with imaging technologies, they are able to target disease states and other anatomies within the human body [2]. Robotic systems enable the surgeon to perform the procedure with dexterity in areas which might not be possible with bare hands. Their combination with imaging technologies have the potential to improve planning, execution, outcome and effectiveness of the intervention [3]. Due to technological progress, improvements in medical imaging and a growing acceptance by surgeons and patients, new use cases for medical robots are regularly being generated [4].

The combination of 3-dimensional (3D) pre or intra-operative imaging data allows robots to precisely guide instruments to anatomical structures [6], [1]. Imaging techniques include 3D modalities such as Computed Tomography (CT) [18] and Magnetic Resonance Imaging (MRI) [19], and 2-dimensional (2D) techniques such as ultrasonography [16] and X-ray fluoroscopy [8]. They reveal the precise location of desired pathologies which can then be used to guide the robot to this location [6]. Such image guided MIS approaches to accurately navigate the robot, requires the robot to be registered to the medical imaging system. The process of registration of a medical robot to the imaging system without the use of any tracking device or continuous X-ray imaging is the core of this work.

Since the introduction of robots to MIS, extensive work has been done to register robots to the imaging systems, for e.g. for robotic needle placement [7], [14], [15]. Various methods for robot assisted instrument targeting under fluoroscopy exist: these robot-image registration algorithms compute the position of the target with respect to the instrument and the geometrical parameters of the imaging system [8], [9]. Such methods use spatial radio-opaque markers distributed on a defined pattern [8], [10]. In [8], a robot targeting method using a marker on the robot end-effector under portable X-ray fluoroscopy based on image servoing is used. Methods to introduce a surgical cooperative system for needle placement using a serial robot for manipulation of biopsy and / or treatment needles has also been described in [14], in which retro-reflecting spheres are attached to the robot and the patient phantom which are tracked with an optical tracking system which is fixed to the C-arm X-ray imaging system. In [11] the automatic positioning of a surgical instrument mounted on a robot end-effector on the basis of visual servoing is presented. However, in prior research regarding robot assisted image guided interventions, basic limitations of tracking systems such as either visibility of markers, line of sight problem, continuous X-ray imaging or complexity of registration algorithms prevail during the registration between the robot and the imaging systems which make the registration constrained and dependent.

In this paper, we propose a method to register a robotic system to an imaging system without the use of a tracking device or X-ray imaging. The registration is realized by pointing the robot to distinct landmarks whose positions are known in the coordinate system of the imaging system. By driving the robot to these distinct landmarks, their position relative to the robot coordinate system is also known and hence the two systems can be registered to each other. To realize this approach, the robot is programmed to work semi-

autonomously: in a man-machine-interface operation mode in which the robotic arm can be moved and guided by the operator by pulling or pushing its structure. This operation mode is referred to as a free floating hand-guided operation mode in the rest of the paper. This approach is further presented in this contribution.

The paper is organized as follows: Section II describes the system architecture with the robotic system, the tool holder and the components of the imaging system. The registration method along with the workflow is also explained in the second part of Section II. In Section III, the experiments and evaluation are demonstrated. The experimental results are discussed in section IV followed by the discussion in section V. Finally, an outlook of further developments concludes this article.

II. MATERIALS AND METHODS

A. System Architecture

Modern interventional radiology suites consist of angiographic flat detector (FD) C-arm systems featuring X-ray fluoroscopy (2D) as well as cone beam CT (CB-CT) for 3D imaging. They are floor mounted or ceiling mounted X-ray systems. Recent C-arm systems even use industrial robots to position the C-arm along the patient.

Fig. 1 shows the main components of the experimental setup which include the multi-axis robot-driven angiographic C-arm X-ray imaging system equipped with a flat-panel detector for image acquisition and the operating table[3]. The setup includes the 7-axes Lightweight robot - "intelligent industrial work assistant"[4] (LWR iiwa) on whose end-effector a customized tool holder is attached. The robotic system is mounted on a customized mobile platform for positioning.
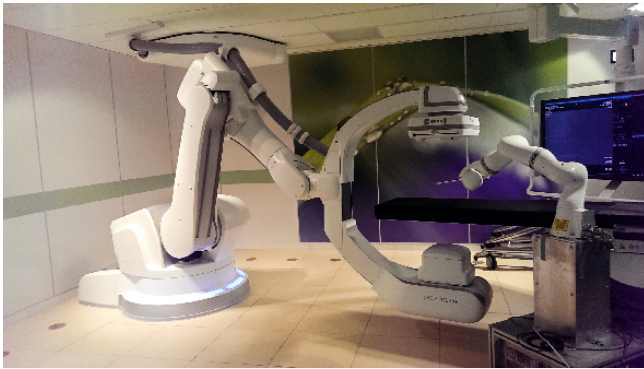

Fig. 1.   System setup with the multi-axis robot-driven angiographic C-arm X-ray imaging system equipped with a flat-panel detector, the LWR and the tool holder attached to it.

1) Coordinate Systems: Multiple coordinate systems as shown in Fig. 2 are defined: the World coordinate system (WCS) located at the foot of the operating table, the Angiography coordinate system (ACS) located at the base of the

robot-driven C-arm system, the Imaging coordinate system (ICS) located in the middle of the head side of the operating table, the Robot base coordinate system (RBCS) located at the robot base, Robot wrist coordinate system (RWCS) located at the mounting flange (the robot wrist where the tool is to be mounted) and the Tool coordinate system (TCS) which is the coordinate system of the tool located at the Tool Center Point (TCP). The origin of the TCS coincides with the TCP which is located at the distal end of the tool. The x, y and z axes of the coordinate systems are shown in red, green and blue colors in Fig. 2.

The ACS and the ICS, which form a part of the WCS have a definite transformation among each other and with the WCS. The transformations WCS to ACS and ACS to ICS represented by T_{WCS}^{ACS} and T_{ACS}^{ICS} respectively are already known in the angiography system i.e. in the WCS.

There are two ways to register the LWR to the C-Arm imaging system. Either by determining the position and orientation of the TCS in the ICS i.e. the transformation represented by T_{ICS}^{TCS} or by determining the position and orientation of the RBCS in WCS represented by T_{WCS}^{RBCS}. In either case, once the transformation of the RBCS in WCS or the TCS in ICS is determined, its position and orientation in all other coordinate systems can be computed.
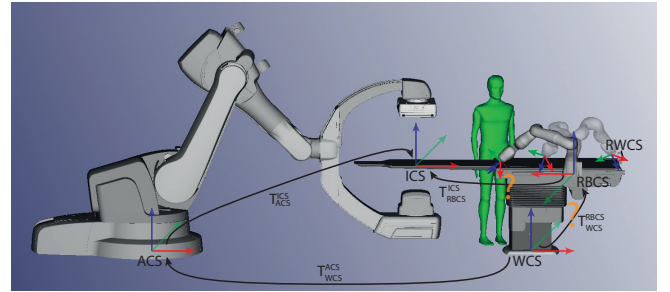

Fig. 2.   The coordinate systems of the interventional suite.

Based on internal torque sensors, the LWR is programmed in the free floating hand-guided operating mode in which it enables the operator to manipulate the robot by manually holding and guiding it by means of haptic interaction along appropriate trajectories to the desired target. This operation mode already takes into account the weight of the LWR, and the weight and the center of mass of the tool attached to its end-effector. It retains its current position once the operator stops applying any external force on it in this operation mode.

2) Tool: The tool holder is mounted on the end-effector of the LWR as shown in Fig. 3. It contains an adapter for a cylindrical tube made of Poly(methyl methacrylate)(PMMA) which has a sharp distal end which is used to point it to the distinct landmarks.

The transformation of the TCS in the RWCS represented by T_{RWCS}^{TCS}, for the cylindrical tube is determined by using another tool, the location of whose TCP in RWCS and thus the transformation T_{RWCS}^{TCS} is already known. T_{RBCS}^{TCS} represents

the transformation of the TCP in the RBCS of this tool when its distal end is manually driven to a distinct landmark in the free floating hand-guided operation mode. T_{RBCS}^{RWCS} represents the transformation of the RWCS in the RBCS when the distal end of the cylindrical tube is driven to the same landmark in the same operation mode. By using these transformations of both the TCP and the RWCS in RBCS at the same landmark and by applying (1),

$$T_{RWCS}^{TCS} = (T_{RBCS}^{RWCS})^{-1} * T_{RBCS}^{TCS} \qquad (1)$$

the transformation T_{RWCS}^{TCS} and hence the TCP of the cylindrical tube is determined.
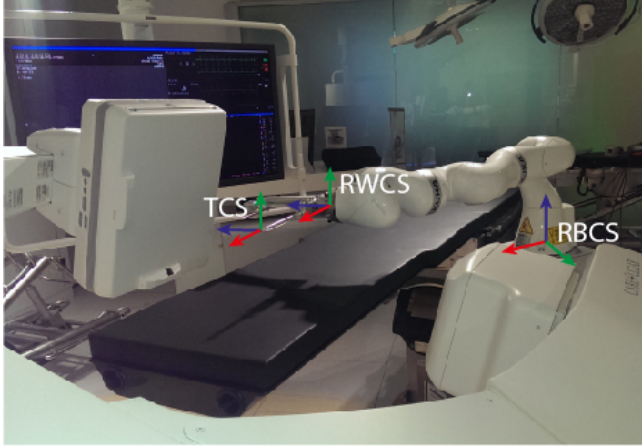

Fig. 3. The tool holder consisting of the cylindrical tube used for the registration process mounted on the end-effector of the LWR and with various coordinate systems associated with it.

3) Registration Landmarks: As shown in Fig. 4 [13], 'A' and 'B' represent the corresponding set of landmarks in the two coordinate systems RBCS and WCS respectively. T_{AB} is the Rigid Body Transformation (RBT) which consists of a rotation matrix **R** and a translation vector **t** applied to the landmark set A to align it with the landmark set B. Here, A and B are defined as [21],

$$A = \{P_A^i\}, \quad \text{for } i = 1 \ldots N \qquad (2)$$

$$B = \{P_B^i\}, \quad \text{for } i = 1 \ldots N \qquad (3)$$

where P_A and P_B are the coordinates of the landmarks in landmark set A and B respectively and N ($N \geq 3$) is the total number of landmarks in A and B.

Generalizing $\{P_A^i\}$ and $\{P_B^i\}$, P is defined as,

$$P = \begin{bmatrix} x \\ y \\ z \end{bmatrix} \qquad (4)$$

and for each landmark, the following equations determine the rotation and translation,
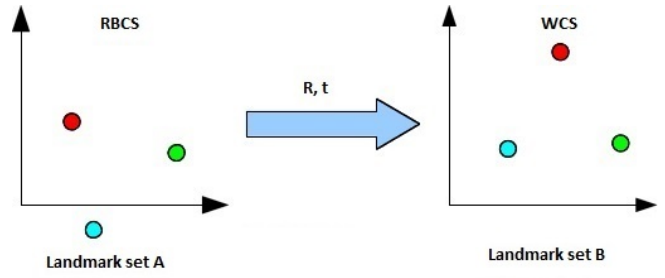
$$P_B = T_{AB} * P_A \qquad (5)$$

Fig. 4. Landmark sets with distinct landmarks in the two coordinate systems RBCS and WCS.

where, T_{AB} is the transformation from landmark set A to B consisting of rotation matrix **R** and translation vector **t**. Hence,

$$P_B = \mathbf{R} * P_A + \mathbf{t} \qquad (6)$$

The aim is to find an optimal solution for **R** and **t** for all coordinates of the landmarks in the landmark set. This leads to the following minimization problem statement [21],

$$\underset{(\mathbf{R},\mathbf{t})}{\arg\min} (\sum_{i=1}^{N} \|P_B^i - \mathbf{R} * P_A^i + \mathbf{t}\|^2) \qquad (7)$$

This transformation T_{AB} between the two sets of landmarks can be determined by using the centroids of the landmark sets as follows [21]:

$$centroid_A = \frac{1}{N} \sum_{i=1}^{N} P_A^i \qquad (8)$$

$$centroid_B = \frac{1}{N} \sum_{i=1}^{N} P_B^i \qquad (9)$$

These centroids are re-centered to the origin of their respective coordinate systems to find the optimal rotation between them using singular value decomposition (SVD) [21],

$$H = \sum_{i=1}^{N} [(P_A^i - centroid_A)(P_B^i - centroid_B)^T] \qquad (10)$$

$$H = USV \qquad (11)$$

where, 'U' and 'V' are (m x m) and (m x n) unitary matrices respectively and 'S' is a (m x n) diagonal matrix. Here m and n are arbitrary dimensions [20]. Then the rotation is given by,

$$R = VU^T \qquad (12)$$

and the translation is given by,

$$t = -R * centroid_A + centroid_B \qquad (13)$$

From the above equations, the transformation,

$$T_{WCS}^{RBCS} = [\mathbf{R} \quad \mathbf{t}] \qquad (14)$$

can hence be determined.

The landmarks for the registration of the LWR to the C-arm imaging system can be distinct screws, holes, edges or
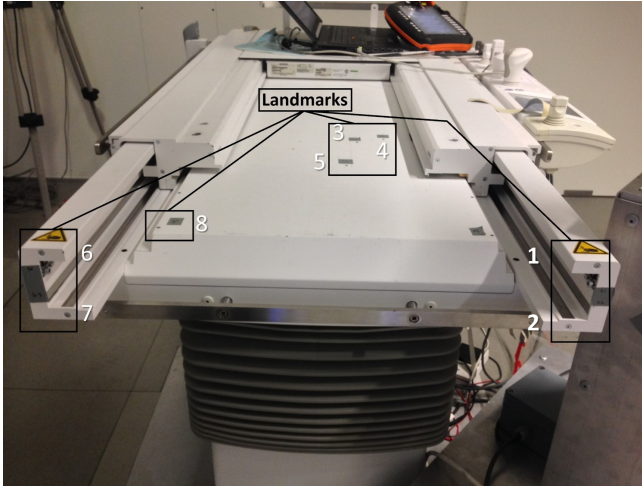
Fig. 5. The distinct landmarks (screws) on the operating table considered for the registration process.

distinct patterns which are known in the WCS. They can be considered to be on the C-arm, the flat-panel detector, the X-ray tube, the operating table or on any other external device whose coordinates are known in the WCS.

In our registration approach, we have considered distinct screws on the operating table as shown in Fig. 5, whose position is known in the WCS. The position of these landmarks in the WCS is read from the Computer-Aided Design (CAD) model of the operating table. Once the position of these landmarks is known in the WCS as well as the RBCS, the transformation between the WCS and the RBCS can be estimated, thereby registering the robot to the C-arm imaging system.

B. Registration Workflow

For the registration process, the LWR is programmed in the free floating hand-guided operating mode and the cylindrical tube is attached to the tool holder mounted on the end-effector of robot. The position and orientation of the TCP in the RWCS represented by the transformation T_{RWCS}^{TCS} is already calculated as explained in section II-A.2.

Once the mobile platform on which the LWR is mounted is moved inside the interventional suite and fixed at one position, the distal end of the cylindrical tube is manually driven using the free floating hand-guided operation mode of the robot to the landmarks on the operating table. The distal end of the tube needs to be in contact with the same point on the landmarks of whose transformation is available from the CAD model. At every landmark, the position and orientation of the TCP of the cylindrical tube in the RBCS is recorded. Once the transformation of all the landmarks in the RBCS is known, it is compared with the transformation of the respective landmarks in the WCS obtained from the CAD model. Using (12) and (13), the relation between the RBCS and the WCS is determined, hence registering the LWR to the C-arm imaging system.

III. EXPERIMENTS

According to the workflow explained in section II-B, the transformation T_{WCS}^{RBCS} using the above mentioned system of equations is determined for the set of 8 landmarks located on the operating table. This workflow is performed for 5 sequences for one fixed position of the mobile platform on which the robot is mounted. The transformation T_{WCS}^{RBCS} is determined for each of the 5 sequences with 8 landmarks and also for multiple combinations of 3 to 8 landmarks for every sequence. This is then used to determine the transformation T_{WCS}^{TCS} for each sequence with 8 landmarks and for every combination of landmarks using (15),

$$(T_{WCS}^{TCS})_i = (T_{WCS}^{RBCS})_i \cdot (T_{RBCS}^{TCS}), \quad \text{for} \quad i = 1 \dots M \quad (15)$$

where M is the number of sequences. This transformation is then individually compared to the ground truth.

A. Ground Truth

A volumetric FD CB-CT of the cylindrical tube including the TCS is acquired by the C-arm system. The tube is segmented on the basis of contrast detection in 397 slices of CB-CT reconstruction and its position and orientation in the ICS is determined as shown in Fig. 6. Once the position and orientation of the TCS in the ICS is determined and the transformation T_{ICS}^{TCS} is estimated, the transformation T_{WCS}^{TCS} is calculated using (16),

$$(T_{WCS}^{TCS})_{gt} = (T_{WCS}^{ICS}) \cdot (T_{ICS}^{TCS})_{gt} \quad (16)$$

where 'gt' represents the ground truth and the transformation T_{WCS}^{ICS} is already known in the angiography system.

The position of the TCS in the WCS derived from the ICS is considered the ground truth, since it is closest to the diagnostic dataset used in clinical applications.
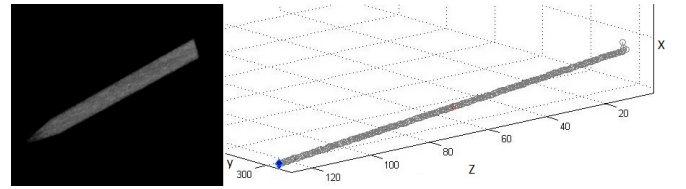

Fig. 6. Ground truth computation: (Left) shows the volume rendered FD CB-CT of the cylindrical tube and (Right) shows the segmentation of the tube in the imaging volume.

IV. RESULTS

For 5 sequences of the registration run considering 8 landmarks located on the operating table, values for the position of the TCS in the WCS are obtained. These values are compared to the ground truth to determine the absolute error, median error, and standard deviation of the position of the TCS in WCS.

When compared to the ground truth for the position of the TCS in WCS, the following absolute error (in mm) as shown in Table I is obtained.

TABLE I
ABSOLUTE ERROR - POSITION OF TCS IN WCS

Axes	Error - position of TCS in WCS in [mm]				
	Seq. 1	Seq. 2	Seq. 3	Seq. 4	Seq. 5
x	13.8	6.9	7.5	7.2	10.1
y	22.6	20.6	16.1	21.6	21.5
z	17.1	18.6	14.4	15.1	19.7

The rms error for each of the 5 sequences is calculated using (17),

$$Error_{rms} = \sqrt{((x_{gt} - x_c)^2 + (y_{gt} - y_c)^2 + (z_{gt} - z_c)^2)} \quad (17)$$

where x_{gt}, y_{gt}, z_{gt} are the ground truth values and x_c, y_c, z_c are the calculated values using landmark transformation. The median of the rms error of all 5 sequences results in a median error of [6.9, 20.6, 18.6] mm i.e. for Seq. 2 and a standard deviation of [2.9, 2.6, 2.2] mm.

For each sequence, various combinations of 3 to 8 landmarks are considered which result in a total number of 't' combinations given by (18),

$$t = \sum_{k=3}^{N} \binom{8}{k} \quad (18)$$

where, 'k' represents the number of landmarks considered. Each combination is used to determine the position of the TCS in the WCS and is compared to the ground truth to evaluate the absolute error.

The rms error for each combination of landmarks is calculated by (17). The mean of the rms error of all combination of landmarks for all 5 sequences, represented by $\overline{Error_{rms}}$ is calculated by (19),

$$\overline{Error_{rms_j}} = \frac{1}{M} \sum_{i=1}^{M} Error_{rms_{i,j}} \quad for \ j = 1 \ldots t \quad (19)$$

where 'j' represents the combination number. Fig. 7 shows the plot of this $\overline{Error_{rms}}$ grouped by the number of landmarks used for registration.

To get an overview of the how reasonable each landmark for the registration process is, we evaluated the registration accuracy for every landmark individually. The normalized sum of all $\overline{Error_{rms}}$ to which a distinct landmark contributes is used. This is illustrated in Fig. 8.

V. DISCUSSION

In the 5 measurement sequences implemented for landmark transformation, a median error of [6.9, 20.6, 18.6] mm i.e. for Seq. 2 and a standard deviation of [2.9, 2.6, 2.2] mm is achieved when compared to the ground truth. A relatively high absolute error is recorded in axes y and z as compared to axis x for all 5 sequences. From both these observations, it can be inferred that a systematic error in axes y and z of the WCS is present. This error may result from inaccurate pointing of the cylindrical tube to the landmarks and inappropriate robot position relative to the landmark positions.
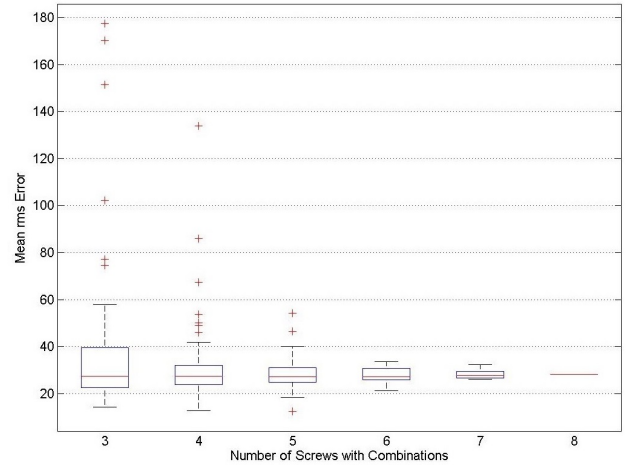

Fig. 7. Mean rms error of all combinations of landmarks for 5 sequences of registration.
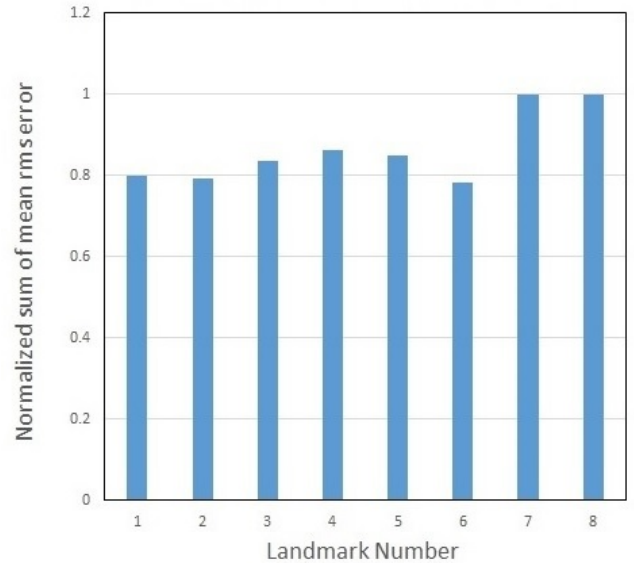

Fig. 8. Normalized mean rms error for all combination of landmarks.

Various combinations of 3 to 8 landmarks for each sequence are considered for evaluating the optimal transformation between the two coordinate systems. It can be observed from Fig. 7 that the range of the rms error significantly decreases as the number of used landmarks increase. A higher number of used landmarks decrease the error range and improves the probability of achieving a reasonable result. Fig. 7 also shows that the median of the mean rms error over the group of 3 to 8 landmarks continuously varies about 1.2 mm. This implies good stability and robustness of the approach followed in this paper.

According to Fig. 8, we observe that landmarks number 7

and 8 out of all the landmarks contribute relatively more to the mean rms error. Considering this observation, we evaluated the landmark transformation procedure explained above excluding landmark number 7 and/or 8. For the combinations of 3 to 6 and/or 3 to 7 landmarks, no improvement in the registration result could be observed. However, the high error value of landmark number 7 and 8 is due to the outliers in the mean rms error of the combinations of 3 and 4 landmarks. Hence, we can conclude that no landmark contributes to better or worse results and should be preferred over the other landmark for the registration approach presented here.

VI. CONCLUSIONS AND OUTLOOK

We present an approach to register a robotic system to a medical imaging system using rigid body transformation based on landmarks known in the coordinate system of the imaging system. Hence, no tracking device which induces limitations such as visibility of markers or line of sight, is used. It also requires less hardware which may lead to lower cost. In medical settings, the robotic system can also be registered to anatomical structures in the patient using the proposed registration technique. Although registration of the robotic system is possible using the imaging system itself, the presented registration approach is desired since it does not use X-ray imaging and therefore is a dose saving technique. This is relevant since the registration may be repeated after relocation of the the mobile platform on which the robot is mounted or if the tool mounted on the robot wrist is changed.

For improving the accuracy of this registration approach, investigation of the systematic error present in axes y and z can be done. Also, by considering the landmarks with a specific geometry such as a definite pattern to obtain more information from each landmark (for e.g. position and orientation), the workflow can be improved. This could lead to better results with lesser number of landmarks. After initial registration, the accuracy of the proposed approach relies on the state estimation of the robotic arm which will further be investigated. Not only in case of medical settings, this registration approach can be extended to other robotic environments as well where tracking devices need to be spared.

REFERENCES

[1] S. R. Kantelhardt, R. Martinez, S. Baerwinkel, R. Burger, A. Giese and V. Rohde "Perioperative course and accuracy of screw positioning in conventional, open robotic-guided and percutaneous robotic-guided, pedicle screw placement," European Spine Journal vol. 20, no. 6, pp. 860-868, 20011.

[2] K. Cleary, A. Melzer, V. Watson, G. Kronreif and D. Stoianovici, "Interventional robotic systems: applications and technology state-of-the-art," Minimally Invasive Therapy & Allied Technologies vol. 15, no. 2, pp. 101-113, 2006.

[3] A.F. Jolesz, "Intraoperative imaging and image-guided therapy," Springer Science & Business Media, 2014.

[4] R. A. Beasley, "Medical robots: Current systems and research directions," Journal of Robotics, 2012.

[5] S. Bann, M. Khan, J. Hernandez, Y. Munz, K. Moorthy, V. Datta, T. Rockall, and A. Darzi, "Robotics in surgery," Journal of the American College of Surgeons, vol. 196, no. 5, pp. 784-795, 2003.

[6] R. D. Howe and Y. Matsuoka, "Robotics for surgery," Annual Review of Biomedical Engineering, vol. 1, no. 1, pp. 211-240, 1999.

[7] R. H. Taylor and D. Stoianovici, "Medical robotics in computer-integrated surgery," IEEE Transactions on Robotics and Automation, vol. 19, no. 5, pp. 765- 781, 2003.

[8] A. Patriciu, et al. "Motion-based robotic instrument targeting under C-Arm fluoroscopy," Medical Image Computing and Computer-Assisted Intervention - MICCAI, pp. 988-998, 2000.

[9] J. Yao, et al. "A progressive cut refinement scheme for revision total hip replacement surgery using C-arm fluoroscopy," Medical Image Computing and Computer-Assisted Intervention - MICCAI, pp. 1010-1019, 1999.

[10] A. Bzostek, et al. "An automated system for precise percutaneous access of the renal collecting system," CVRMed - MRCAS, pp. 299-308, 1997.

[11] A. Krupa, et al. "Autonomous 3-D positioning of surgical instruments in robotized laparoscopic surgery using visual servoing," IEEE Transactions on Robotics and Automation, vol. 19, no. 5, pp. 842-853, 2003.

[12] R. Bischoff, J. Kurth, G. Schreiber, R. Koeppe, A. Albu-Schäffer, A. Beyer, O. Eiberger, S. Haddadin, A. Stemmer, G. Grunwald, et al., "The kuka-dlr lightweight robot arm - a new reference platform for robotics research and manufacturing," Joint 41th International Symposium on Robotics and 6th German Conference on Robotics, pp. 1-8, VDE, 2010.

[13] N. Ho, "Finding optimal rotation and translation between corresponding 3D points," http://nghiaho.com/?page_id=671.

[14] S. Tovar-Arriaga, R. Tita, J. C. Pedraza-Ortega, E. Gorrostieta, and W. A. Kalender,"Development of a robotic fd-ct-guided navigation system for needle placement - preliminary accuracy tests," The International Journal of Medical Robotics and Computer Assisted Surgery, vol. 7, no. 2, pp. 225-236, 2011.

[15] D. Stoianovici, L.L. Whitcomb, J. H. Anderson, R. H. Taylor and L. R. Kavoussi, "A modular surgical robotic system for image guided percutaneous procedures," Medical Image Computing and Computer-Assisted Intervention - MICCAI, pp. 404-410, 1998.

[16] J. Hong, T. Dohi, M. Hashizume, K. K. Mokoto and N. Hata, "An ultrasound-driven needle-insertion robot for percutaneous cholecystostomy," Physics in Medicine and Biology, vol. 49, no. 3, pp. 441, 2004.

[17] Dreval, O. N., I. P. Kasparova, K. A. Bruskin, A. Aleksandrovskii and V. Zil'bernstein "Results of using spine assist mazor in surgical treatment of spine disorders," interventions (transpedicular fixations), vol. 5, no. 6, pp. 9-22, 2014.

[18] J. Brodie and S. Eljamel, "Evaluation of a neurosurgical robotic system to make accurate burr holes," The International Journal of Medical Robotics and Computer Assisted Surgery, vol.7, no. 1, pp. 101-106, 2011.

[19] J. Tokuda, et al. "Integrated navigation and control software system for MRI-guided robotic prostate interventions," Computerized Medical Imaging and Graphics vol. 34, no. 1, pp. 3-8, 2010.

[20] L. N. Trefethen and D. Bau III, "Numerical linear algebra," Vol. 50, Siam, 1997.

[21] A. K. Somani, T. S. Huang and S. D. Blostein, "Least-squares fitting of two 3-D point sets," IEEE Transactions on Pattern Analysis and Machine Intelligence, no. 5, pp. 698-700, 1987.